Efficient photoactivatable Dre recombinase for cell type-specific spatiotemporal control of genome engineering in the mouse

Huiying Li[a,1], Qiansen Zhang[a,1], Yiran Gu[b,1], Yingyin Wu[a], Yamei Wang[b], Liren Wang[a], Shijie Feng[b], Yaqiang Hu[a], Yansen Zheng[a], Yongmei Li[a], Haifeng Ye[a], Bin Zhou[c], Longnian Lin[b], Mingyao Liu[a,2], Huaiyu Yang[a,2], and Dali Li[a,2]

[a]Shanghai Key Laboratory of Regulatory Biology, Institute of Biomedical Sciences and School of Life Sciences, East China Normal University, Shanghai 200241, China; [b]Key Laboratory of Brain Functional Genomics (Ministry of Education), Institute of Brain Functional Genomics, East China Normal University, Shanghai 200062, China; and [c]State Key Laboratory of Cell Biology, Chinese Academy of Sciences Center for Excellence in Molecular Cell Science, Shanghai Institute of Biochemistry and Cell Biology, Chinese Academy of Sciences, University of Chinese Academy of Sciences, Shanghai 200031, China

Edited by Lei Wang, University of California San Francisco Medical Center, San Francisco, CA, and accepted by Editorial Board Member Tak W. Mak November 11, 2020 (received for review March 2, 2020)

Precise genetic engineering in specific cell types within an intact organism is intriguing yet challenging, especially in a spatiotemporal manner without the interference caused by chemical inducers. Here we engineered a photoactivatable Dre recombinase based on the identification of an optimal split site and demonstrated that it efficiently regulated transgene expression in mouse tissues spatiotemporally upon blue light illumination. Moreover, through a double-floxed inverted open reading frame strategy, we developed a Cre-activated light-inducible Dre (CALID) system. Taking advantage of well-defined cell-type–specific promoters or a well-established Cre transgenic mouse strain, we demonstrated that the CALID system was able to activate endogenous reporter expression for either bulk or sparse labeling of CaMKIIα-positive excitatory neurons and parvalbumin interneurons in the brain. This flexible and tunable system could be a powerful tool for the dissection and modulation of developmental and genetic complexity in a wide range of biological systems.

optogenetics | photoactivatable Dre recombinase | cell labeling

Precisely defining, visualizing, or modulating cellular signaling pathways in specific cell types via genetic engineering methods is intriguing and challenging (1). With the identification and optimization of genome engineering enzymes, advances in genetic technologies have opened up new avenues not only for labeling distinct cell types but also for dissection of gene functions in intact animals (2). Site-specific recombinases, especially tyrosine-recombinase family members such as Cre (3) and Flp (4), play pivotal roles in genome engineering due to their high specificity and efficiency. These recombinases enable deletion, integration, inversion, as well as translocation of genomic DNA without the assistance of accessory proteins. Among them, Cre recombinase is the most frequently used tool for mouse genetics because of its remarkable efficiency. During the past few decades, the development of a series of inducible Cre recombinase systems has substantially improved the strength and spectrum of the technology. For example, chemically inducible systems such as CreER (5), DiCre (6), and DD-Cre (7) enable temporally specific activation of the recombinase through small molecule-mediated recombinase translocation, dimerization, or stabilization. Moreover, light-inducible systems [e.g., CRY2-CIB1-PA-Cre (8), Magnets-PA-Cre (9)] have been developed to elegantly manipulate the genome in a spatiotemporal manner in cultured cells and, more importantly, in multiple mouse tissues such as the liver and brain (10). These tools based on Cre recombinase have demonstrated a wide variety of applications, but a single recombinase system has technical hurdles that constrain the development of elaborate genetic models for understanding complicated biological process.

Dre recombinase, derived from bacteriophage D6, is one of the most widely used site-specific recombinases. It recognizes a 32-bp target site rox and does not cross-react with other tyrosine-recombinase family members (11). Recently, several rox variants have been developed (12) based on a Dre-dependent double-floxed inverted open reading frame (DIO) system, enabling a broader range of specific recombinations. Like Cre recombinase, the Dre-rox system has been demonstrated to be highly efficient in *Escherichia coli* and mammalian cells, as well as in mice (13). In addition, Dre has no obvious toxicity during development (14). With high activity and functioning orthogonally to Cre, Dre has proven to be a very good player together with Cre in setting up dual-recombinase systems for sophisticated genome engineering. For example, our recent studies have demonstrated that dual-recombinase–activated lineage tracing enhanced the precision of Cre-mediated lineage tracing and provided accurate evidence to illuminate some debates about cell origin (15, 16). As with Cre recombinase, ligand-inducible Dre systems have been

Significance

Precisely defining specific cell types is critical but challenging for biological studies. Site-specific tyrosine-recombinase Cre and its inducible variants have been widely used in efficient genetic engineering. However, a single recombinase system has technical hurdles. Here, a photoactivatable Dre (PA-Dre) recombinase is developed by tethering split Dre fragments to the light-inducible Magnets system. PA-Dre is efficient and stringently controlled in vitro and in vivo. Moreover, with the creation of the Cre-activated light-inducible Dre system, it is able to achieve bulk or sparse labeling of specific neurons in a spatiotemporal manner. This flexible and tunable system could be adapted to a wide range of biological systems for the modulation of developmental and genetic complexity.

Author contributions: H.L., M.L., H. Yang, and D.L. designed research; H.L., Q.Z., Y.G., Y. Wu, Y. Wang, L.W., S.F., Y.H., Y.Z., Y.L., and H. Yang performed research; B.Z. contributed new reagents/analytic tools; H.L., Q.Z., H. Ye, B.Z., L.L., H. Yang, and D.L. analyzed data; and H.L., Q.Z., and D.L. wrote the paper.

Competing interest statement: The authors have submitted a patent application (application number 201910759889.4) based on the results reported in this study.

This article is a PNAS Direct Submission. L.W. is a guest editor invited by the Editorial Board.

[1]H.L., Q.Z., Y.G. contributed equally to this work.

[2]To whom correspondence may be addressed. Email: myliu@bio.ecnu.edu.cn, hyyang@bio.ecnu.edu.cn, or dlli@bio.ecnu.edu.cn.

This article contains supporting information online at https://www.pnas.org/lookup/suppl/doi:10.1073/pnas.2003991117/-/DCSupplemental.

First published December 14, 2020.

developed through fusion of Dre with progesterone receptor or estrogen receptor, which exhibit good ligand-responsive induction properties (17). However, these chemical-inducible systems have obvious limitations. For example, inducible recombinase-mediated sparse labeling can be achieved by lowering the recombinase activity through titrating the dose of inducer, but the optimal concentration is not easily attained, and a chemically induced system is unable to directly label the cells of interest with a high spatiotemporal resolution.

To generate an advanced inducible Dre system, we sought to develop a highly efficient photoactivatable Dre recombinase (PA-Dre). In this light-inducible system, Dre recombinase was split into two complementary N- and C-terminal fragments. Each split Dre fragment was attached to nMag and pMag, respectively, which separately lack Dre activity. In the presence of blue light, the two complementary split Dre fragments are brought together by the light-activated dimerization system, allowing recombination. Here, based on the similarity with the structure of Cre, and with computational assistance, we performed a thorough screening of potential split sites in the Dre primary sequence and identified three inducible split Dre pairs ($DreN_{60}$/$DreC_{61}$, $DreN_{150}$/$DreC_{151}$, and $DreN_{246}$/$DreC_{247}$). Among these, $DreN_{246}$/$DreC_{247}$ showed high efficiency and stringent regulation of gene expression. Through a series of optimization steps, we designed a highly efficient PA-Dre and demonstrated its light-dependent recombination activity in mammalian cells and in mice. Furthermore, to facilitate broader applications of PA-Dre, we generated a Cre-activated light-inducible Dre (CALID) system and specifically achieved sparse and bulk labeling of the neurons in the mouse brain. Taken together, we add another set of efficient tools to the genomic toolbox, which will enable more detailed investigations of different cell populations through

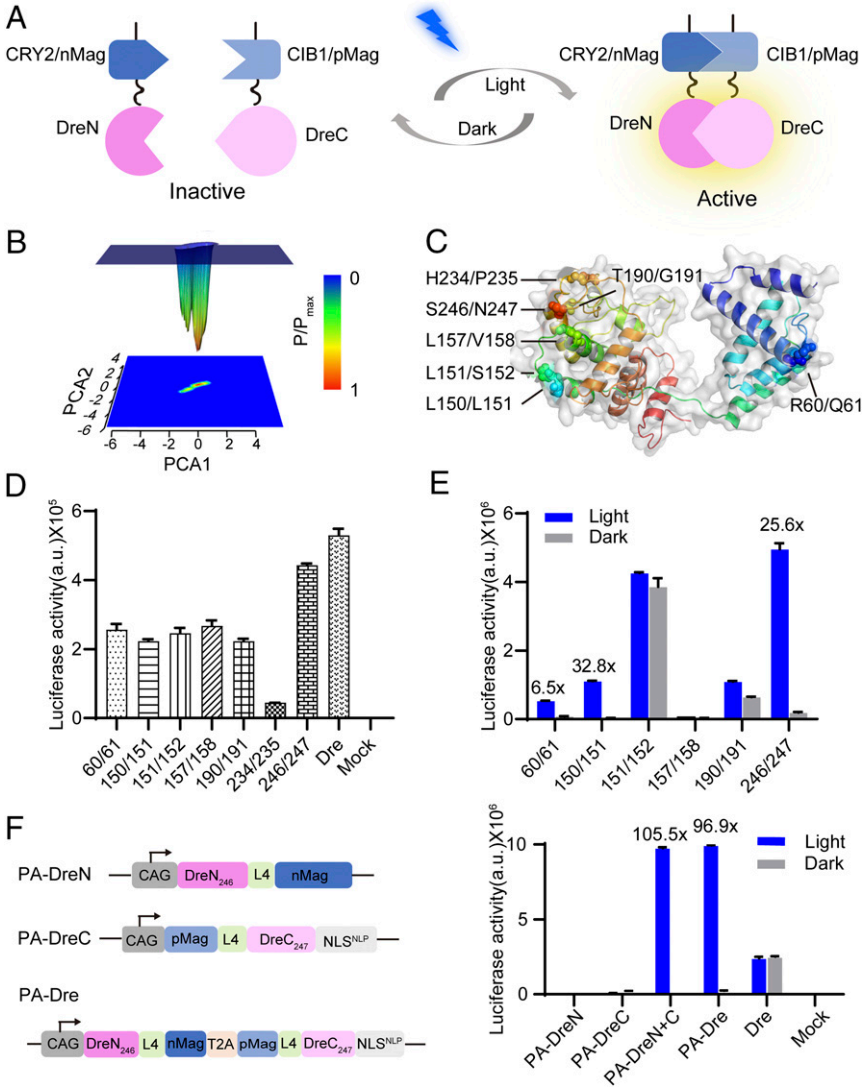

Fig. 1. Generation and optimization of the PA-Dre system. (*A*) Schematic diagram of the PA-Dre system functional mechanism. (*B*) Probability map of the MD snapshots with PCA1 and PCA2 as coordinates. The probability of the most abundant conformation is set to 1, and the relative probabilities of other conformations with respect to this conformation are shown. (*C*) Representative conformation of the state with the highest probability. Split sites designed on the basis of this conformation are marked in the figure. (*D*) Luciferase assay of various DreN-Coh2/DreC-Docs pairs with indicated split sites using the rox-stop-rox-Rluc reporter in HEK-293T cells. (*E*) Luciferase reporter assay for evaluating the recombination efficiency of various DreN-nMag/DreC-pMag constructs in HEK-293T cells with or without illumination. (*F*) Construction of PA-Dre in a single plasmid. Schematic representation using T2A peptide to generate the PA-Dre system in a single plasmid. Luciferase reporter assay was performed in HEK-293T cells with or without illumination. The empty vector (mock) along with rox-stop-rox-RLuc was used as a negative control. The full-length Dre recombinase in a similar amount was used as a positive control. The results in *D*–*F* are shown as the mean ± SD of $n = 3$ independent experiments.

high-spatiotemporal-resolution and cell type-specific genetic manipulation. Moreover, we believe that photoactivatable Dre recombinase, along with already existing Cre driver mouse lines, may be useful in broad fields of biology, such as specific cellular ablation and tissue regeneration, increasing our understanding of the roles of specific cell populations in the near future.

Results

Computational Design and Screening of Split Dre. To develop a PA-Dre, we speculated that a two-component system could be more flexible for extensive optimization, especially to reduce background activity. Ideally, in light-inducible systems [for example, CRY2-CIB1 (18) or Magnets system (19)], two split Dre segments could be functionally restored in the presence of light (Fig. 1*A*). Since the possible sites for splitting Dre recombinase into individually nonfunctional halves have not yet been reported, we first empirically selected nine possible split sites based on two optimized Cre split positions ($CreN_{59}$/$CreC_{60}$ and $CreN_{104}$/$CreC_{106}$) (6). To simplify the screening system, the cohesion–dockerin pair (a high-affinity protein–protein interaction) was used as dimerization module (20) (*SI Appendix*, Fig. S1*A*). The corresponding DreN–Coh2 and DreC–Docs pairs were transfected into human embryonic kidney (HEK)-293T cells together with a Renilla luciferase reporter (rox-stop-rox-Rluc). The reporter became activated once Dre recombinase deleted a transcriptional stop sequence flanked by two rox sites (*SI Appendix*, Fig. S1*B*). To our surprise, only $DreN_{60}$/$DreC_{61}$ fused to the Coh2–Docs system exhibited significant, but not strong, recombinase activity (*SI Appendix*, Fig. S1*C*). Next, the CRY2–CIB1 system was employed to generate photoactivatable Dre recombinase through fusion with $DreN_{60}$ and $DreC_{61}$ fragments, respectively (*SI Appendix*, Fig. S1*D*). However, the CRY2–CIB1-based Dre system only exhibited slight recombinase activity after illumination compared with full-length Dre recombinase (*SI Appendix*, Fig. S1*E*), suggesting this split site was not suitable for light-inducible Dre recombinase.

In order to find optimal Dre split sites, we applied a series of computer-assisted protein design methods. Since no crystal structure of Dre was available, we first built a Dre structural model using homology modeling based on Cre recombinase [Protein Data Bank (PDB) code 1F44] (21), which displayed 41% similarity to Dre recombinase via the SWISS-MODEL workspace (22) (*SI Appendix*, Fig. S2). Dre functions through binding with corresponding DNA substrates, which would further stabilize the structure when forming a DNA/protein complex. Next, we performed molecular dynamic (MD) simulation to optimize the Dre model in the presence of DNA based on the crystal structure of the Cre–DNA complex (PDB code 1F44) (21). An MD simulation system was constructed (*SI Appendix*, Fig. S3*A*), and a 200-ns MD simulation was carried out for further optimization. The principal component analysis (PCA) (23) suggested that the first two ranking principal components represent the major movement trends, as they covered almost 67% of the trajectory, while the values decreased monotonically after this point (*SI Appendix*, Fig. S3*B*). We then employed PCA for clustering the obtained MD trajectory and identified that the Dre model was stable, as it was mainly concentrated in one state during the MD simulation (Fig. 1*B*). Based on the representative Dre structure from the MD simulation, we predicted new Dre split sites according to two criteria: 1) selecting interface residues between the loop structure and the α helix or the corner of the loop structure and avoiding selecting residues inside the α helix, as this should minimize disruption of the protein folding structure; and 2) avoiding splitting at residues mediating contact between Dre and DNA in order to reduce the interference with DNA binding due to the split site. In total, six new Dre split sites were selected for testing (Fig. 1*C*). Highly consistent with the six selected sites, these were also acquired by SPELL (24) based on the Dre model from the MD simulation, indicating our split strategy was feasible.

In the second round of screening, five of the six split Dre pairs exhibited similar or higher recombinase activity compared with $DreN_{60}$/$DreC_{61}$ in the noninducible Coh2–Docs dimerization system. The assembly of $DreN_{246}$/$DreC_{247}$ halves exhibited comparable enzyme activity with full-length Dre construct, suggesting its good performance (Fig. 1*D*). Then, the five pairs of the split Dre halves were conjugated to the CRY2–CIB1-based light-induced system. However, only $DreN_{150}$/$DreC_{151}$ showed ∼10-fold reporter induction in HEK-293T cells in response to blue light stimulation (*SI Appendix*, Fig. S4*A*). We speculated that, due to the large sizes of CRY2 (∼70 kDa) and CIB1(∼37 kDa), the 3D structure of the dimerized CRY2–CIB1 might create a steric hindrance that blocks the split Dre from reconstituting properly. Therefore, we turned to the much smaller one, the Magnets system (17.1 kDa). Strikingly, the Magnets system exhibited much better performance than the CRY2–CIB1 system, especially on $DreN_{246}$/$DreC_{247}$, which showed 25.6-fold induction after illumination (Fig.1*E*). Hence, we decided to use the Magnets system as the photoswitch to further optimize the $DreN_{60}$/$DreC_{61}$, $DreN_{150}$/$DreC_{151}$, and $DreN_{246}$/$DreC_{247}$ halves to generate an outperforming PA-Dre. We also compared pulse (Fig.1*E*) or continuous (*SI Appendix*, Fig. S4*B*) illumination treatment, and no obvious difference was observed. Thus, pulse illumination was employed in all subsequent experiments.

Development and Optimization of PA-Dre. First, different orientations of the Dre fragments relative to the nMag/pMag domains were tested. Consistently, for all three combinations of split Dre halves, the combination DreN–nMag and pMag–DreC exhibited the highest induction, suggesting this orientation was optimal for Magnets photoswitch-controlled Dre activity (*SI Appendix*, Fig. S5*A*). Due to the much lower recombination efficiency of $DreN_{60}$/$DreC_{61}$, the $DreN_{150}$/$DreC_{151}$ and $DreN_{246}$/$DreC_{247}$ split Dre pairs were used for further optimization. As the linker sequence was critical for the activity of fusion proteins, six different flexible or rigid linkers from the literature (25, 26) or created by our group were tested. We found that the L4 linker dramatically decreased the background activity but did not affect recombination activity after illumination for both $DreN_{150}$/$DreC_{151}$ and $DreN_{246}$/$DreC_{247}$ (>70-fold induction; *SI Appendix*, Fig. S5*B*). To further decrease the background activity, we hypothesized that distinct subcellular localization of the Dre/Mag halves would be effective. Thus, variants of $DreN_{246}$–nMag and pMag–$DreC_{247}$ with or without nuclear localization sequence (NLS) from the simian virus 40 (SV40) large T antigen (NLS^{SV40}) were constructed (*SI Appendix*, Fig. S5*C*). As expected, the induction effects were significantly increased when NLS was added to only one of the Dre/Mag halves. In particular, the combination of $DreN_{246}$–nMag and pMag–$DreC_{247}$–NLS^{SV40} showed about ∼83-fold induction (*SI Appendix*, Fig. S5*D*). In order to further improve the nuclear entry efficiency of pMag–$DreC_{247}$–NLS^{SV40} upon exposure to blue light, we replaced the NLS^{SV40} with three strong variant NLS sequences (27), respectively. Notably, the NLS derived from nucleoplasmin (NLS^{NLP}) exhibited the highest fold induction when it was fused to the C terminus of $DreC_{247}$ (*SI Appendix*, Fig. S5 *E–G*). Next, we attempted to create an all-in-one vector through linking the optimized $DreN_{246}$–nMag (PA-DreN) and pMag–$DreC_{247}$–NLS^{NLP} (PA-DreC) with two different self-cleaving 2A peptides (*SI Appendix*, Fig. S5*H*). We found that the PA-Dre construct using T2A peptide, which is known to have lower self-cleavage efficiency than P2A (28), exhibited slightly lower recombination activity but higher induction fold than P2A peptide construct (*SI Appendix*, Fig. S5 *H* and *I*). Substitution of a T2A mutant ($T2A_{mut}$) sequence with impaired cleavage efficiency (29) led to reduced recombination efficiency but did not increase background activity, suggesting

that uncleaved PA-Dre was not active with or without light induction (*SI Appendix*, Fig. S5 *H* and *I*). As a result of these successive improvements, we obtained a PA-Dre construct which showed the highest light-dependent recombinase activity of ~100-fold induction (Fig. 1*F*). Interestingly, the activity of PA-Dre was even much higher (~4.5-fold) than the wild type Dre driven by a CAG promoter when similar molar mass of plasmid DNA was transfected. We speculate that fusion of the Magnets system makes the split Dre more flexible and form a conformation with higher activity.

To further investigate the structural basis for efficient PA-Dre function, all-atom MD simulations were conducted. MD simulations of PA-Dre/DNA were carried out with a focus on the structural dynamics of $DreN_{246}/DreC_{247}$ interacting with DNA. Two independent 200-ns MD simulations were performed with different initial velocities. The weak rmsd values of PA-Dre and DNA indicated that there was no large structural variation detected by the simulations (*SI Appendix*, Fig. S6*A*). Moreover, no significant conformational change was found in either Dre split or DNA in both the initial and final snapshots. We also analyzed the distance between the Ser246 and Asn247 Cα atoms. The distance is stable during the two parallel simulations, indicating that there is no large change in Dre split sites between Ser246 and Asn247 (*SI Appendix*, Fig. S6*B*). Taken together, the above simulation results suggest that PA-Dre can work efficiently by stably binding to DNA in a manner similar to full-length Dre. Given this information, we speculated that split Dre could also be used with other dimerization systems. Four inducible reassembly systems, the blue-light system [the fungal photoreceptor Vivid (VVD)] (30), the red-light system (PhyB-PIF3) (31), the near-infrared light system (Bphp1-Q-PAS1) (32), and a chemical switch (FKBP-FRB) (33), were investigated and confirmed (*SI Appendix*, Fig. S7*A*). These results suggest that the S246/N247 split Dre pair is applicable for a variety of dimerization systems, especially VVD, since the Magnets system is derived from VVD (19) (*SI Appendix*, Fig. S7*B*).

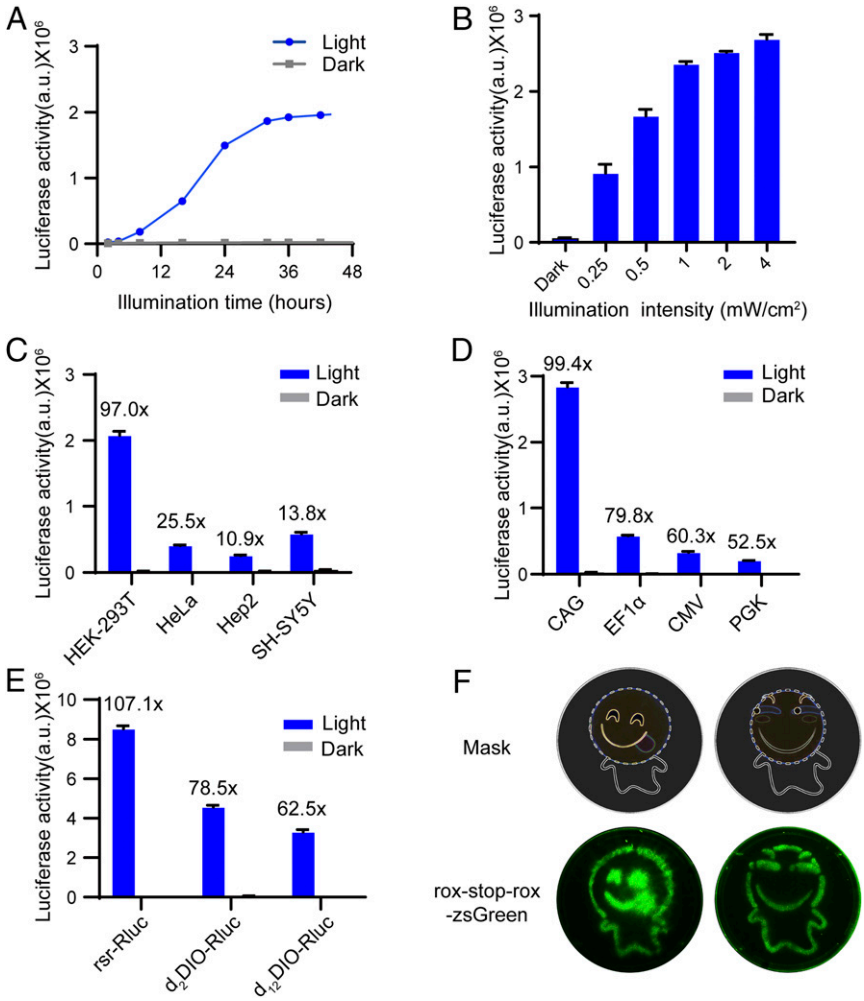

Fig. 2. Detailed characterization of PA-Dre in vitro. (*A*) Exposure time-dependent PA-Dre activity. HEK-293T cells were transfected with PA-Dre and the rox-stop-rox-RLuc reporter. The cells were illuminated for indicated times, and the luciferase activity was determined. (*B*) Exposure intensity-dependent PA-Dre activity. HEK-293T cells were transfected with PA-Dre and rox-stop-rox-RLuc reporter. The cells were illuminated for indicated intensity, and then the luciferase activity was determined. The results in *A* and *B* are shown as the mean ± SD of $n = 4$ independent experiments. (*C*) PA-Dre activity in distinct cell types. HEK-293T, HeLa, Hep2, and SH-SY5Y cells were transfected with PA-Dre and rox-stop-rox-RLuc reporter. Luciferase activity was determined in these cells with or without illumination. (*D*) Determination of PA-Dre activity under the control of variant promoters. PA-Dre constructs driven by indicated promoters were cotransfected with the rox-stop-rox-RLuc reporter in HEK-293T cells. Luciferase activities were determined in these cells with or without illumination. (*E*) Graph of catalytic activity of PA-Dre for three Rluc reporters. The structure of reporter plasmids is shown in *SI Appendix*, Fig. S10; rox2 and rox12 are rox variants. The results in *C*–*E* are shown as the mean ± SD of $n = 3$ independent experiments. (*F*) Spatially controlled gene activation by PA-Dre. HEK-293T cells were transfected with PA-Dre and rox-stop-rox-zsGreen reporter. The cells were illuminated with blue light for 24 h from the bottom of the dishes, which were covered by a carved photomask (*Top*), resulting in a corresponding pattern of zsGreen expression (*Bottom*).

Characterization of PA-Dre In Vitro. To further characterize the performance of PA-Dre, illumination time and intensity responsiveness were meticulously investigated. HEK-293T cells transfected with PA-Dre and the rox-stop-rox-RLuc reporter were exposed to light for different durations or kept in the dark. As expected, Rluc activities were maintained at undetectable levels in the dark. Reporter activity significantly increased by illumination for 4 to 32 h and then reached saturation (Fig. 2*A*). Moreover, PA-Dre responded very well to blue light intensity as tested from 0.25 to 4 mW/cm^2 and reached maximum level at 1 mW/cm^2, which contributed to reducing potential phototoxicity (34) (Fig. 2*B*). Similar results were also obtained when the reporter was changed to CMV-rox-stop-rox-zsGreen, suggesting that the activity of PA-Dre was time- and intensity-dependent on blue light illumination (*SI Appendix*, Figs. S8 and S9). Additionally, we found that PA-Dre functioned very well in a number of mammalian cell lines with different tissue origins (Fig. 2*C*). Almost undetectable background activity and very strong induction after illumination were observed once the PA-Dre coding region was driven by a distinct strong promoter (35), suggesting that PA-Dre was compatible with variant promoters (Fig. 2*D*). PA-Dre also efficiently catalyzed recombination of several mutant rox sequences (12, 36) to induce a Dre-dependent double-floxed inverted open reading frame upon illumination (Fig. 2*E* and *SI Appendix*, Fig. S10). Importantly, one of the unique advantages of a light-control system is accurate spatial induction control. As shown in Fig. 2*F*, blue light precisely activated PA-Dre to induce rox-stop-rox-zsGreen reporter expression in culture dishes covered with 3D-printed photomasks (Fig. 2*F* and *SI Appendix*, Fig. S11). Taken together, these results demonstrate that PA-Dre is an efficient light-inducible recombinase, which is tunable for precise spatiotemporal transgene activation in vitro.

Photoactivation of Gene Expression In Vivo via PA-Dre. The tightly controlled features as well as the robustness of PA-Dre upon illumination in cell culture encouraged us to investigate this system in vivo. The plasmids expressing PA-Dre and rox-stop-rox-FLuc (firefly luciferase) were systemically delivered into wild type mouse livers via hydrodynamic tail vein (HTV) injection (37) (Fig. 3*A*). The mice were illuminated with blue light at the indicated duration 8 h postinjection or kept in the dark, and the luciferase activity was examined 24 h after injection (Fig. 3*B*). Similar to cell cultures, 30-min illumination induced a significant luciferase activity, which was further increased upon longer illumination (Fig. 3*C*). In order to verify whether PA-Dre enables DNA recombination in vivo with minimal duration of illumination, we found that PA-Dre–mediated recombination was achieved by short periods of illumination (~30 s) with increased amounts of plasmids injected (Fig. 3*D*). These results demonstrated that PA-Dre can efficiently mediate recombination in vivo even with minimal duration of illumination. To directly compare PA-Dre with Magnets–PA-Cre in vivo, these two systems were individually injected with a luciferase reporter into mice through HTV. The procedure and injected DNA amount strictly followed a previous report (9) (*SI Appendix*, Fig. S12*A*). PA-Dre showed much higher fold induction (91.8-fold vs. 9.1-fold) but lower luciferase reporter activity than Magnets–PA-Cre (*SI Appendix*, Fig. S12 *B* and *C*). When the recombinase DNA amount was increased to a higher dose, both of the recombinase systems exhibited similar efficiency but PA-Dre induced much lower background activity (*SI Appendix*, Fig. S12*D*). It was not due to different spontaneous leakage between these two reporter systems after detailed comparison through in vitro and in vivo examinations (*SI Appendix*, Fig. S12 *E* and *F*), suggesting PA-Dre was more stringent than Magnets–PA-Cre in vivo.

Efficient Genetic Labeling in Mouse Tissues by PA-Dre Delivered by Adeno-Associated Viral Vectors. To test whether the PA-Dre system could be adapted to use in potent recombinant adeno-associated viral (AAV) vectors for efficient genetic labeling, PA-Dre was packaged into a hepatocyte-tropic AAV8 virus and delivered into adult R26-RSR-tdTomato mice (38) through tail vein injection (Fig. 4*A*). We observed that light-dependent tdTomato expression was mainly in livers from illuminated mice. Moreover, the recombination efficiency of PA-Dre was tunable through varying the amount of AAV injection (Fig. 4*B*), with very low background activity (Fig. 4*C*). Consistent with a previous report (39), the fluorescence from tdTomato proteins was mainly observed at the lower edge of the liver, since the majority of the tissue was covered by the thorax, which blocked illumination. The blue light penetrated the liver tissue for about 900 μm with the indicated light intensity (Fig. 4*D*).

Optogenetics is a very critical methodology in neuroscience. To evaluate our PA-Dre in the mouse hippocampal region, AAV9 virus expressing PA-Dre was delivered into the dorsal CA1 of R26-RSR-tdTomato mice (Fig. 4*E*). Similar to the validation of the PA-Dre system in mouse liver, robust fluorescence was observed in the mice that received illumination, but no background activity was detected in the control mice without light stimulation. Moreover, increased light intensity also led to higher PA-Dre activity, which induced a larger area of tdTomato expression (Fig. 4*F*). These results suggested that PA-Dre was able to achieve efficient genetic labeling through AAV vectors with very tightly controlled illumination responsiveness in living mouse tissues.

Cre-Dependent PA-Dre Activation for Bulk and Sparse Labeling in the Mouse Brain. Light-induced Cre or Dre recombinases are powerful tools for spatiotemporal control, but it is difficult to achieve photo-switchable activity in a cell type-specific manner. To generate a cell type-specific PA-Dre system, we leveraged the Cre-dependent DIO strategy and developed the Cre-activated light-inducible Dre (CALID) system, which was functional exclusively in Cre-expression cells. Theoretically, P1 and P2 are distinct cell type-specific promoters driving Cre and floxed inverted PA-Dre, respectively. Cre restores the orientation of PA-Dre, which activates the rox site flanked gene of interest (GOI) in P1 and P2 double-positive cells after illumination, which elegantly defines the cells under triple-positive conditions (Fig. 5*A*). Since numerous tissue-specific Cre strains have been generated, the CALID system could be widely used in a cell type-specific manner for light-dependent genetic manipulation. For our proof-of-principle study, AAV9 vectors encoding CALID along with CaMKIIα-EGFP-2A-Cre were delivered into the hippocampal dentate gyrus (DG) of adult R26-RSR-tdTomato mice (Fig. 5*B*). One week after injection, the mice were illuminated via the implanted optical fibers (Fig. 5*C*). As expected, tdTomato expression was only observed in Cre-positive neurons in illuminated mice but not in controls. Moreover, to achieve sparse or bulk labeling of the excitatory neurons, mice receiving 1-s or 5-min illumination were compared. The data demonstrated that the number of labeled neurons was positively correlated with the illumination time, suggesting the CALID system was accurately tunable in the mouse brain (Fig. 5*D*).

To test the spatiotemporal cell type-specific genetic labeling in an existing Cre strain, parvalbumin (PV)-Cre mice (40) were bred with the R26-RSR-tdTomato strain, and the resulting offspring were injected with AAV9-CALID and AAV9-CMV-EGFP (for injection indication) into the medial prefrontal cortex (mPFC; Fig. 5*E*). One week after injection, the mice were illuminated via the implanted optical fiber (15 mW/cm^2, 1 s). The identity of PV neurons was confirmed via immunofluorescence staining with PV antibody. As expected, a small-diameter (100-μm) optical fiber induced sparse labeling in PV neurons, and

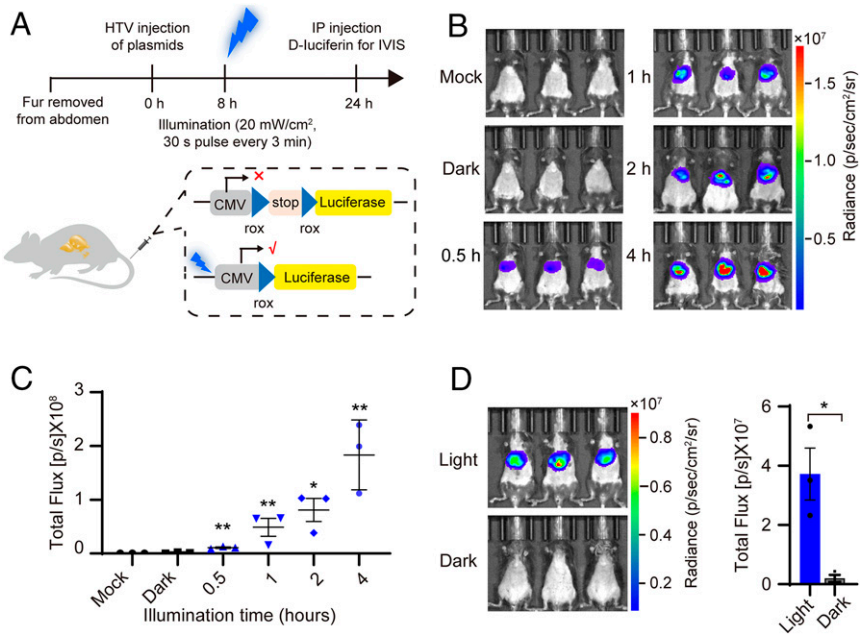

Fig. 3. Light activation of exogenous reporter in vivo. (*A*) Schematic diagram of the procedure used to treat the wild type mice with PA-Dre plasmids. PA-Dre and rox-stop-rox-Fluc reporter plasmids were delivered through HTV, and the luciferase activity was determined within 10 min after D-luciferin injection. (*B*) The luciferase activity was determined in low-dosage group mice ($n = 3$ mice per group) with or without illumination for indicated durations. (*C*) Quantification of the bioluminescence images obtained in *B*. (*D*) The luciferase activity was determined in high-dosage group mice ($n = 3$ mice per group) with illumination for 30 s or darkness. Quantification of the bioluminescence images are presented (*Right*). The results in *C* and *D* are shown as the mean ± SD; statistical analysis was calculated by Student's *t* test; $n = 3$ mice (*$P < 0.05$, **$P < 0.01$ versus dark control).

bulk labeling was achieved by using a large-diameter (200-μm) optical fiber using the same illumination time and intensity parameters (Fig. 5*F*). These data demonstrate that the CALID system, through AAV or combined with Cre-expressing mouse strains, is able to achieve cell type-specific spatiotemporal manipulation of genome recombination in living animals.

Discussion

Tyrosine site-specific recombinases are powerful genome engineering enzymes that are able to efficiently and precisely modify DNA. With the development of remotely controllable systems, the applications of these critical enzymes have been robustly improved in developmental and synthetic biology, as well as in biomedical research (41). In this study, we focused on the generation of a photoactivated PA-Dre system and demonstrated its outstanding performance both in cell culture and in animals. Moreover, with the development of the CALID system, we were able to achieve photo-switchable cell type-specific spatiotemporal manipulation of genome recombination in living animals.

Dre recombinase is a reliable tool and has been widely used for genome engineering, especially combined with Cre due to their orthogonality. However, inducible Dre systems are not well established, particularly the light-inducible system, which has several advantages against chemical or photocaged systems (9). In this study, a light-inducible protein association system was employed due to its quick response to stimulation. However, it is critical and challenging to identify effective protein split sites that lack significant spontaneous assembly, which would increase the protein-of-interest background activity. Based on computational design, we identified several split sites that retained high activity upon reassembly. The $DreN_{246}/DreC_{247}$ split site was adaptable to both photoswitchable (VVD, PhyB-PIF3, and BphP1-Q-PAS1) and chemical-inducible (FRB-FKBP) systems, suggesting it is generally compatible with a wide range of inducible systems. The $DreN_{151}/DreC_{152}$ site exhibits strong spontaneous reassembly activity, which is useful for other controllable systems. For example, using two distinct promoters to drive individual halves of Dre would enable cell-type definition by multiple features similar to intersectional labeling (42).

To reduce the basal activity and increase the induction response, we optimized the relative directional configuration, the linker amino acid sequence, and the nuclear localization signal. The maximum induction ratio of PA-Dre reached more than 100-fold after step-by-step molecular optimization. Unexpectedly, we accidentally discovered a linker (L4) due to incorrect cloning of the L6, $(SGGS)_2$–XTEN–(SGGS) linker (25), which can reduce the background of PA-Dre by more than 40 fold. It will be interesting to test whether this linker outperforms in other fusion protein systems. Compared with Magnets–PA-Cre, PA-Dre exhibited much stringent response to light induction in vivo, especially at higher dose (*SI Appendix*, Fig. S12*D*). It is a very important feature for exogenous delivery of light-inducible recombinase system, since it will be more tolerant to variation of the amount of DNA injected either through naked DNA or recombinant viruses.

Precisely defining and visualizing specific cell types is an intriguing and challenging task. The INTronic Recombinase Sites Enabling Combinatorial Targeting system (36) and the dual-AAV sparse labeling system (43) are powerful tools for genetic intervention and observation in living animals. However, these systems are barely controlled by viral injection, which requires empirical optimization for each application, especially for sparse labeling. The CALID system developed in this study integrated the blue lights as a trigger, which is more flexibly and tightly controllable by instruments. With the CALID system, it is easy to activate a target gene in the whole hippocampus for bulk labeling or a few neurons for sparse labeling in a spatiotemporal manner. The CALID system could also be evolved for more stringent labeling and genetic modulation through two specific promoters to drive the expression of Cre (or CreERT2) and PA-Dre

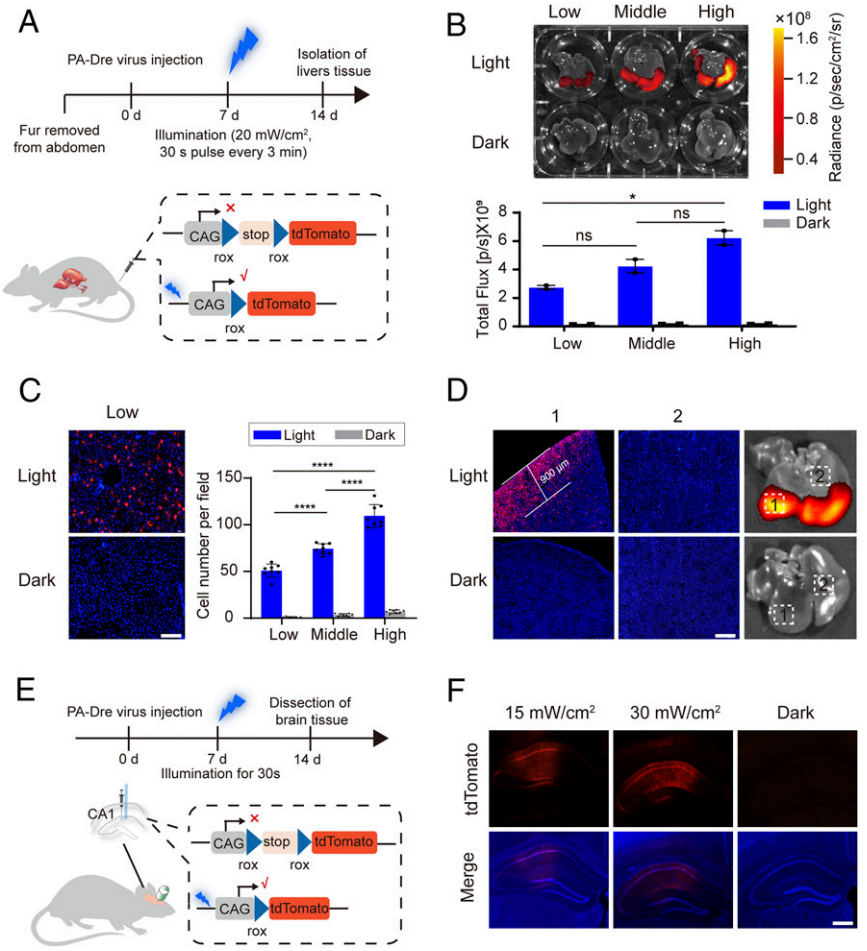

Fig. 4. Activation of endogenous reporter in mouse liver and brain. (*A*) Schematic diagram of the procedure used to treat heterozygous R26-RSR-tdTomato reporter mice with AAV8 PA-Dre in mouse liver. (*B*) Bioluminescence images of isolated liver tissue from the mice injected with different titer viruses (low-titer, 1.25×10^{11} vg; middle-titer, 2.5×10^{11} vg; and high-titer, 5×10^{11}; $n = 2$ mice per group) with or without illumination. The results are shown as the mean ± SD; statistical analysis was calculated by Student's *t* test; $n = 2$ mice (*$P < 0.05$; ns, not significant). (*C*) Fluorescence images of liver sections from the group that received low-titer AAV injection (*Left*). (Scale bar, 100 μm.) Statistics of tdTomato-positive cell number per field from liver tissues that received low, middle, or high titers of PA-Dre AAV treatments (*Right*). Graph represents the quantification of tdTomato-positive cells in coronal slices in each group. The results are shown as the mean ± SD of $n = 8$ slices. Statistical analysis was calculated by Student's *t* test (****$P < 0.0001$). (*D*) Fluorescence images of sections at the indicated positions in liver tissues from mice that received low-titer PA-Dre AAV injection. (Scale bar, 500 μm.) (*E*) Schematic diagram of the procedure used to treat heterozygous R26-RSR-tdTomato reporter mice with AAV9 PA-Dre in mouse dorsal hippocampal CA1 region. (*F*) Fluorescent images of the dorsal CA1 sections of the mice injected with AAV-PA-Dre with or without illumination. The mice were implanted with optical fibers over CA1, which were exposed to blue light for 30 s with the indicated intensity 1 wk post viral injection. Control animals were kept in darkness without illumination. (Scale bar, 500 μm.) DAPI (blue) indicates the stained nucleus, and tdTomato appears red.

individually within these two-promoter double-positive cell populations.

Here we developed a photoactivatable Dre recombinase system and an adapted CALID system for highly efficient, tunable, and spatiotemporal control of transgene expression and cell labeling. We believe that, with the development of a stable transgenic CALID mouse strain, more broad applications could be achieved in multiple systems once crossed with numerous existing Cre transgenic mouse models.

Materials and Methods

Plasmid Construction. Split Dre fragments were amplified from the coding sequence of optimized Dre recombinase in our previous study (15). Coh2, Docs, CIB1, CRY2, PhyB, PIF3, nMag, pMag, BphP1, Q-PAS1, FRB, and FKBP cDNA were synthesized by Genewiz. pCAG–DreN–Coh2 and pCAG–DreC–Docs plasmids were ligated into the transposon-bearing plasmid pT2/BH (Addgene no. 26557). The DNA-encoding linker amino acid sequences were synthesized by Genewiz and inserted into indicated constructs. Individual NLS sequence was introduced via Gibson assembly (Vazyme). For construction of CALID, a DNA cassette derived from PA-Dre was constructed in an AAV backbone vector using the DIO strategy. The reporter plasmids, rox-stop-rox-Rluc and rox-stop-rox-Fluc, were inserted into the AAV backbone construct under the control of a CMV promoter. All prepared constructs have been validated by DNA sequencing, and the sequence of PA-Dre and CALID system are listed in *SI Appendix*, Supplementary Notes S1 and S2).

Cell Culture, Transfections, and Illumination. HEK-293T cells (American Type Culture Collection CRL-3216) were cultured in Dulbecco's modified Eagle's medium supplemented with 10% fetal bovine serum (Gibco), 1% penicillin, and streptomycin (Basalmedia) at 37 °C with 5% CO_2 incubation. For the luciferase assay, HEK-293T cells were plated at a density of 1.5×10^5 cells per well in 24-well plates (Corning). The cells were cotransfected with 100 ng of the rox-stop-rox-Rluc reporter and 100 ng of each split Dre recombinase fragment (or PA-Dre) using polyethylenimine (PEI; Polysciences). Twenty-four hours after transfection, the cells were illuminated with blue light (470 ± 20 nm, 1.0 mW/cm², 30-s pulse every 3 min) for 24 h or kept in darkness. For cells transfected with PhyB-PIF3, the medium was changed the next day after transfection with 5 μM phycocyanobilin and illuminated (650 nm, 1.0 mW/cm², 30-s pulse every 3 min) for 24 h or kept in darkness. For the BphP1-Q-PAS1 pair, the cells transfected were illuminated (1.0 mW/cm², 30-s

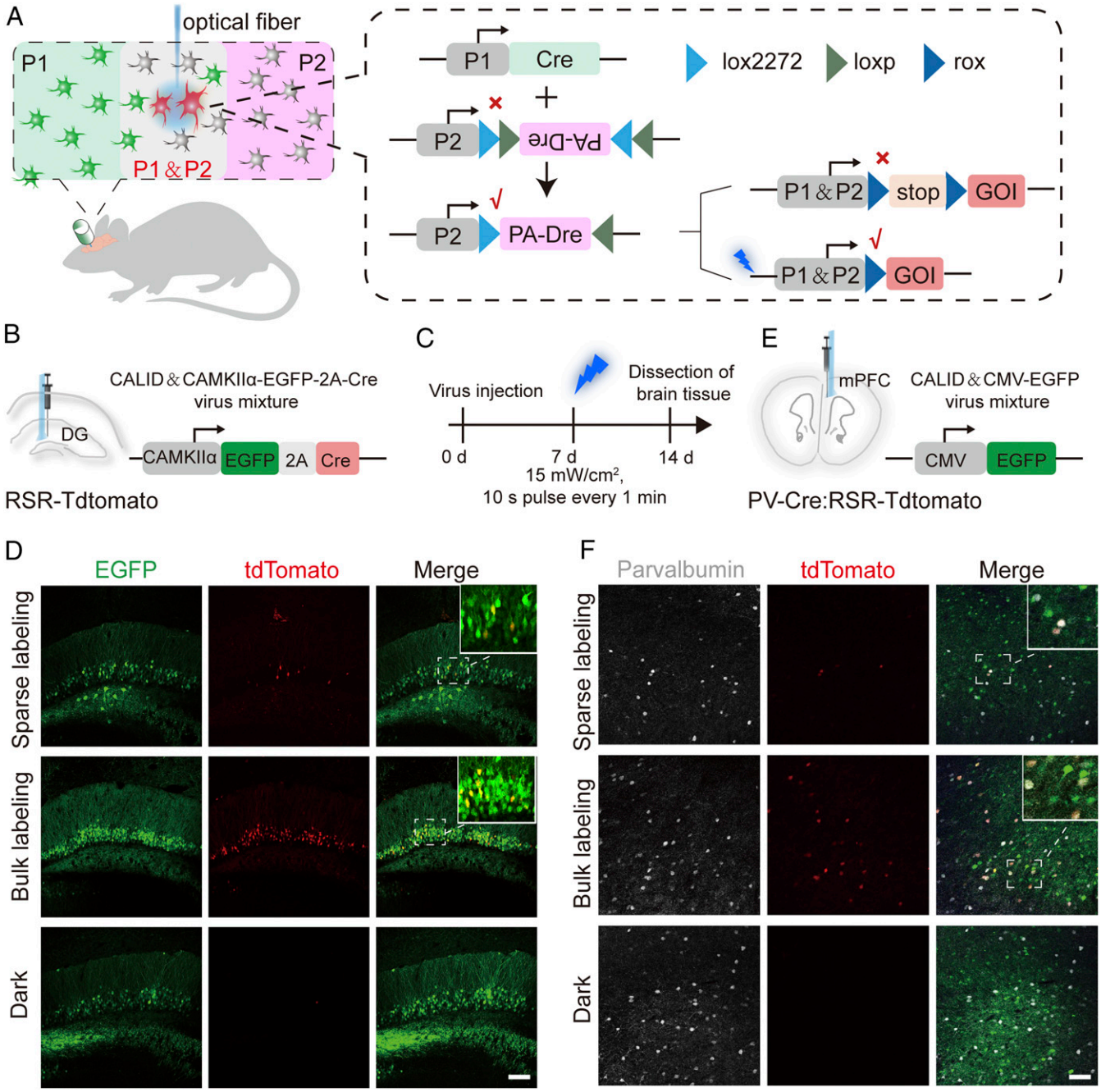

Fig. 5. Labeling of specific neurons in the mouse brain via the CALID system. (*A*) Schematic diagram of the CALID system working theory. P1 and P2 are distinct cell type-specific promoter driving Cre and floxed-PA-Dre, respectively. Cre restores the orientation of PA-Dre, which activates the GOI in P1 and P2 double-positive cells after illumination. (*B*) Schematic of viral injection into the hippocampal DG region of the heterozygous R26-RSR-tdTomato mice ($n = 3$ mice per group). (*C*) Schematic diagram of the procedure used to treat the R26-RSR-tdTomato reporter mice injected with indicated viral vectors. (*D*) Sections of mouse brain injected with virus as shown in *B*. The mice had optical fibers implanted over the hippocampus and were then exposed to blue light for 1 s (for sparse labeling) or 5 min (10-s pulse every 1 min for bulk labeling; top two rows) 1 wk post viral injection. Control animals (bottom row) were kept in darkness without optical fiber illumination. tdTomato (red) expression was observed in Cre/EGFP-positive neurons (green). (Scale bar, 100 μm.) (*E*) Schematic diagram of the procedure used to treat double-heterozygous PV-Cre:R26-RSR-tdTomato mice ($n = 3$ mice per group) injected with indicated AAV vectors encoding CALID and EGFP for visualization. (*F*) Fluorescent images of brain sections from the mice as treated in *E*. Mice were implanted with 100-μm (*Top*) or 200-μm–diameter (*Middle*) optical fibers over the mPFC, which were used to illuminate the mPFC with blue light (15 mW/cm^2, 1 s) 1 wk post injection. Control mice (*Bottom*) were kept in the dark without optical fiber illumination. EGFP (green) indicates the site of injection. PV inhibitory interneurons are shown in white via antibody against PV protein. tdTomato (red) expression was restricted to PV-Cre–positive cells of illuminated mice, but not in control mice. (Scale bar, 100 μm.)

pulse every 3 min) for 24 h or kept in darkness. For rapamycin-induced activation of split Dre, the medium was changed the next day after transfection with 100 nM rapamycin. The luminescence assay was performed with Stop & Glo Reagent (Promega) using a LumiSTAR Omega counter (BMG LabTech) following the manufacturer's instructions. To prove the spatial specificity of PA-Dre, HEK-293T cells were plated on a 10-cm dish covered by a 3D-printed black photomask on the bottom. The cells were cotransfected with PA-Dre (10 μg) and a rox-stop-rox-zsGreen reporter (10 μg) and

illuminated with blue light (470 ± 20 nm, 1.0 mW/cm^2, 30-s pulse every 3 min) for 24 h. Fluorescence images were acquired 24 h after illumination using ChemiScope 4300 Pro imaging equipment (Clinx).

AAV Production. All viruses were packaged and produced in HEK-293T cells. In brief, HEK-293T cells were seeded in a 10-cm dish and transiently transfected with the transfer plasmid (7.5 μg) containing the GOI, AAV serotype plasmid (7.5 μg), and helper plasmid (10 μg) for each dish using PEI (90 μL, 1 μg/μL). At 72 h posttransfection, transfected cells with recombinant AAV particles were collected and further purified using the iodixanol purification method. The titer of recombinant viruses was determined by qPCR and stored at −80 °C until use. Viral titers were 6.5×10^{12} vg/mL for PA-Dre, 7×10^{12} vg/mL for CALID, and 7.2×10^{12} vg/mL for CaMKIIα-EGFP-2A-Cre.

Animals. The mice used in this study were C57/BL6 strain and housed up to four to a standard cage in a specific pathogen-free facility. Adult wild-type mice, R26-RSR-tdTomato mice (38), and PV-Cre (40) mice were kept on a reverse 12-h light/dark cycle with ad libitum food and water. All animal experiments were approved by the East China Normal University Center for Animal Research. Related procedures were performed in accordance with the guidelines drafted by the Association for Assessment and Accreditation of Laboratory Animal Care in Shanghai.

HTV Injection and Reporter Assay in Mice. The abdominal fur of 5-wk-old C57BL/6 mice was shaved, and the mice were randomly divided into two groups: high-dose group (100 μg of the PA-Dre plasmid and 50 μg of the rox-stop-rox-Fluc plasmid) and low-dose group (50 μg of the PA-Dre plasmid and 25 μg of the rox-stop-rox-Fluc). The plasmids in 2 mL of Ringer's buffer were delivered systemically via HTV injection within 5 to 8 s. The mice were kept in the dark or illuminated with an LED light source (20 mW/cm^2, 30-s pulse every 3 min) for each indicated time course. At 24 h after hydrodynamic transfection, the mice were anesthetized with isoflurane. At 5 min after i.p. injection with 100 μL D-luciferin, the mice were examined using an IVIS Spectrum instrument (Caliper Life Sciences). In order to avoid the effects of signal attenuation, images were captured within 10 min of D-luciferin injection.

AAV Injection and Detection of Reporter Activity in R26-RSR-tdTomato Mice. For PA-Dre–induced endogenous gene analysis in the mouse liver, 5-wk-old Dre reporter mice (heterozygous R26-RSR-tdTomato) were injected with AAV8 encoding PA-Dre (1.25×10^{11} vg, 2.5×10^{11} vg, or 5×10^{11} vg for each mouse) in a total volume of 1 mL phosphate-buffered saline (PBS) solution. One week after infection, the mice were kept in the dark or illuminated with an LED light source (20 mW/cm^2, 30-s pulse every 3 min) for 2 h and euthanized 1 wk after light stimulation. For fluorescent imaging, livers were washed with cold PBS and placed in a six-well culture plate. To analyze PA-Dre activity in the mouse brain, R26-RSR-tdTomato mice were anesthetized with pentobarbital sodium (40 mg/kg) and placed in a stereotaxic frame. Brain areas were targeted using coordinates from Paxinos and Franklin's. For viral injection experiments, AAV9 PA-Dre (1.5×10^8 vg) was unilaterally injected in the hippocampal dorsal CA1 region [stereotaxic coordinates from lambda: anterior–posterior (AP), −2.30 mm; medial–lateral (ML), ±2.00 mm; dorsal–ventral (DV), −1.10 mm from skull) to a volume of 0.5 μL using a 5.0-μL Neuros syringe (Hamilton). Optical fibers (DV −0.80 mm from skull) were implanted post injection. Mouse body temperature was kept constant by a small animal thermoregulation device (FHC) during the surgery. One week after infection, the mice were kept in the dark or illuminated with an optical fiber (200-μm diameter; Newdoon) at an intensity of 15 mW/cm^2 or 30 mW/cm^2 for 30 s and euthanized 1 wk after light stimulation.

For validation of the CALID system in the mouse hippocampal DG, heterozygous R26-RSR-tdTomato mice (6 to 8 wk old) were unilaterally injected with two AAV9 vectors (CALID and CaMKIIα-EGFP-2A-Cre, 1:1 ratio, 1×10^8 vg) in hippocampal DG (stereotaxic coordinates from lambda: AP, −2.00 mm; ML, ±1.40 mm; DV, −1.70 mm from skull) to a volume of 0.5 μL using a 5.0-μL Neuros syringe (Hamilton). Optical fibers (DV −1.40 mm from skull) were implanted post injection. Illumination stimulation was started 1 wk after viral injection. Awake and freely moving mice were stimulated via optical fiber (200-μm diameter; DV −1.40 mm from skull) at an intensity of 15 mW/cm^2 for 1 s or 5 min. One week after light stimulation, mice were euthanized and perfused. The dissected brains were subjected to immunohistochemistry. For validation of the CALID system in the mPFC, F1 mice, double-heterozygous, derived from the PV-Cre strain and R26-RSR-tdTomato mice were unilaterally injected with two AAV9 vectors (CALID and CMV-EGFP, 1:1 ratio, 1×10^8 vg) in mPFC (stereotaxic coordinates from lambda: AP, +1.90 mm; ML, ±0.80 mm; DV, −1.70 mm from skull) to a volume of 0.5 μL using a 5.0-μL Neuros syringe (Hamilton). Optical fibers (DV −1.40 mm from skull) were implanted post injection. One week postinjection, awake and freely moving mice were stimulated via optical fiber (100-μm or 200-μm diameter) at an intensity of 15 mW/cm^2 for 1 s.

Histology. For thin liver sections, livers were collected and fixed with 4% PFA for 2 h, followed by dehydration in 15% sucrose overnight at 4 °C. The next day, small pieces of liver tissues were dehydrated in 30% sucrose for 2 to 3 h and then embedded in OCT compound (Leica). The fixed livers were cut into 5-μm sections with a Leica CM 1950 cryostat. For section staining, slices were washed three times with PBS for 5 min to remove OCT. After washing, slices were incubated with PBST (0.2% Triton in PBS) for 10 min at room temperature and mounted with mounting medium (Vector) containing DAPI. For 50-μm brain section staining, brains were isolated after perfusion and incubated overnight in 4% PFA. After washing with cold PBS, the brain sections were sliced in PBS using a vibratome (Leica vt1000s). Then, the slices were gently transferred to a glass slide and mounted with mounting medium with DAPI. The coverslip was carefully placed on each slice. Fluorescence images of all slices were acquired using a confocal microscope (Leica SP8) and analyzed using LAS X software.

Data Analysis. Statistical analyses were performed with Prism 8.0 software (GraphPad). Bioluminescence and fluorescence signal of livers were measured using Living Image 4.4 software (PerkinElmer/Caliper Life Sciences). Fluorescence images derived from a confocal microscope were analyzed using LAS X software.

Data Availability. All study data are included in the article and *SI Appendix*.

ACKNOWLEDGMENTS. We are grateful to Shaochuang Liu (Nanjing University) for his technical assistance with timer-controlled LED devices and Dr. Stefan Siwko (Texas A&M University Health Science Center) for scientific editing of this manuscript. This work was partially supported by grants from National Key R&D Program of China (2019YFA0802800 and 2019YFA0110802), Shanghai Municipal Commission for Science and Technology Grants (20140900200), the National Natural Science Foundation of China (32025023 and 81670470), grants from the Shanghai Municipal Commission for Science and Technology (18411953500) and the Innovation program of Shanghai Municipal Education Commission (2019-01-07-00-05-E00054), the Fundamental Research Funds for the Central Universities, the "XingFuZhiHua" funding of East China Normal University (ECNU; 44300-19311-542500/006), and the support of ECNU Public Platform for innovation (01 and 011).

1. D. P. Doupé, N. Perrimon, Visualizing and manipulating temporal signalling dynamics with fluorescence-based tools. *Sci. Signal.* **7**, re1 (2014).
2. B. H. Weinberg *et al*., High-performance chemical- and light-inducible recombinases in mammalian cells and mice. *Nat. Commun.* **10**, 4845 (2019).
3. N. Sternberg, Bacteriophage P1 site-specific recombination: III. Strand exchange during recombination at lox sites. *J. Mol. Biol.* **150**, 603–608 (1981).
4. K. G. Golic, S. Lindquist, The FLP recombinase of yeast catalyzes site-specific recombination in the Drosophila genome. *Cell* **59**, 499–509 (1989).
5. A. K. Indra *et al*., Temporally-controlled site-specific mutagenesis in the basal layer of the epidermis: Comparison of the recombinase activity of the tamoxifen-inducible Cre-ER(T) and Cre-ER(T2) recombinases. *Nucleic Acids Res.* **27**, 4324–4327 (1999).
6. N. Jullien, F. Sampieri, A. Enjalbert, J. P. Herman, Regulation of Cre recombinase by ligand-induced complementation of inactive fragments. *Nucleic Acids Res.* **31**, e131 (2003).
7. R. Sando 3rd *et al*., Inducible control of gene expression with destabilized Cre. *Nat. Methods* **10**, 1085–1088 (2013).
8. A. Taslimi *et al*., Optimized second-generation CRY2-CIB dimerizers and photoactivatable Cre recombinase. *Nat. Chem. Biol.* **12**, 425–430 (2016).
9. F. Kawano, R. Okazaki, M. Yazawa, M. Sato, A photoactivatable Cre-loxP recombination system for optogenetic genome engineering. *Nat. Chem. Biol.* **12**, 1059–1064 (2016).
10. K. Meador *et al*., Achieving tight control of a photoactivatable Cre recombinase gene switch: New design strategies and functional characterization in mammalian cells and rodent. *Nucleic Acids Res.* **47**, e97 (2019).
11. B. Sauer, J. McDermott, DNA recombination with a heterospecific Cre homolog identified from comparison of the pac-c1 regions of P1-related phages. *Nucleic Acids Res.* **32**, 6086–6095 (2004).
12. K. Chuang, E. Nguyen, Y. Sergeev, T. C. Badea, Novel heterotypic rox sites for combinatorial Dre recombination strategies. *G3 (Bethesda)* **6**, 559–571 (2016).
13. K. Anastassiadis *et al*., Dre recombinase, like Cre, is a highly efficient site-specific recombinase in E. coli, mammalian cells and mice. *Dis. Model. Mech.* **2**, 508–515 (2009).

14. A. Nern, B. D. Pfeiffer, K. Svoboda, G. M. Rubin, Multiple new site-specific recombinases for use in manipulating animal genomes. *Proc. Natl. Acad. Sci. U.S.A.* **108**, 14198–14203 (2011).
15. L. He *et al*., Enhancing the precision of genetic lineage tracing using dual recombinases. *Nat. Med.* **23**, 1488–1498 (2017).
16. Q. Liu *et al*., Lung regeneration by multipotent stem cells residing at the bronchioalveolar-duct junction. *Nat. Genet.* **51**, 728–738 (2019).
17. Y. Wang *et al*., Genetic tracing of hepatocytes in liver homeostasis, injury, and regeneration. *J. Biol. Chem.* **292**, 8594–8604 (2017).
18. M. J. Kennedy *et al*., Rapid blue-light-mediated induction of protein interactions in living cells. *Nat. Methods* **7**, 973–975 (2010).
19. F. Kawano, H. Suzuki, A. Furuya, M. Sato, Engineered pairs of distinct photoswitches for optogenetic control of cellular proteins. *Nat. Commun.* **6**, 6256 (2015).
20. Y. Barak *et al*., Matching fusion protein systems for affinity analysis of two interacting families of proteins: The cohesin-dockerin interaction. *J. Mol. Recognit.* **18**, 491–501 (2005).
21. K. C. Woods, S. S. Martin, V. C. Chu, E. P. Baldwin, Quasi-equivalence in site-specific recombinase structure and function: Crystal structure and activity of trimeric Cre recombinase bound to a three-way Lox DNA junction. *J. Mol. Biol.* **313**, 49–69 (2001).
22. M. Biasini *et al*., SWISS-MODEL: Modelling protein tertiary and quaternary structure using evolutionary information. *Nucleic Acids Res.* **42**, W252–W258 (2014).
23. M. Ringnér, What is principal component analysis? *Nat. Biotechnol.* **26**, 303–304 (2008).
24. O. Dagliyan *et al*., Computational design of chemogenetic and optogenetic split proteins. *Nat. Commun.* **9**, 4042 (2018).
25. N. M. Gaudelli *et al*., Programmable base editing of A•T to G•C in genomic DNA without DNA cleavage. *Nature* **551**, 464–471 (2017).
26. X. Chen, J. L. Zaro, W.-C. Shen, Fusion protein linkers: Property, design and functionality. *Adv. Drug Deliv. Rev.* **65**, 1357–1369 (2013).
27. M. Ray, R. Tang, Z. Jiang, V. M. Rotello, Quantitative tracking of protein trafficking to the nucleus using cytosolic protein delivery by nanoparticle-stabilized nanocapsules. *Bioconjug. Chem.* **26**, 1004–1007 (2015).
28. J. H. Kim *et al*., High cleavage efficiency of a 2A peptide derived from porcine teschovirus-1 in human cell lines, zebrafish and mice. *PLoS One* **6**, e18556 (2011).
29. E. Minskaia, M. D. Ryan, Protein coexpression using FMDV 2A: Effect of "linker" residues. *BioMed Res. Int.* **2013**, 291730 (2013).
30. B. D. Zoltowski *et al*., Conformational switching in the fungal light sensor vivid. *Science* **316**, 1054–1057 (2007).
31. S. Shimizu-Sato, E. Huq, J. M. Tepperman, P. H. Quail, A light-switchable gene promoter system. *Nat. Biotechnol.* **20**, 1041–1044 (2002).
32. T. A. Redchuk, E. S. Omelina, K. G. Chernov, V. V. Verkhusha, Near-infrared optogenetic pair for protein regulation and spectral multiplexing. *Nat. Chem. Biol.* **13**, 633–639 (2017).
33. J. Chen, X. F. Zheng, E. J. Brown, S. L. Schreiber, Identification of an 11-kDa FKBP12-rapamycin-binding domain within the 289-kDa FKBP12-rapamycin-associated protein and characterization of a critical serine residue. *Proc. Natl. Acad. Sci. U.S.A.* **92**, 4947–4951 (1995).
34. M. Mansouri, T. Strittmatter, M. Fussenegger, Light-controlled mammalian cells and their therapeutic applications in synthetic biology. *Adv. Sci. (Weinh.)* **6**, 1800952 (2018).
35. C.-m. Chen, J. Krohn, S. Bhattacharya, B. Davies, A comparison of exogenous promoter activity at the ROSA26 locus using a PhiC31 integrase mediated cassette exchange approach in mouse es cells. *PLoS One* **6**, 6–13 (2011).
36. L. E. Fenno *et al*., Targeting cells with single vectors using multiple-feature Boolean logic. *Nat. Methods* **11**, 763–772 (2014).
37. F. Liu, Y. Song, D. Liu, Hydrodynamics-based transfection in animals by systemic administration of plasmid DNA. *Gene Ther.* **6**, 1258–1266 (1999).
38. L. Madisen *et al*., Transgenic mice for intersectional targeting of neural sensors and effectors with high specificity and performance. *Neuron* **85**, 942–958 (2015).
39. X. Wang, X. Chen, Y. Yang, Spatiotemporal control of gene expression by a light-switchable transgene system. *Nat. Methods* **9**, 266–269 (2012).
40. S. Hippenmeyer *et al*., A developmental switch in the response of DRG neurons to ETS transcription factor signaling. *PLoS Biol.* **3**, e159 (2005).
41. G. Meinke, A. Bohm, J. Hauber, M. T. Pisabarro, F. Buchholz, Cre recombinase and other tyrosine recombinases. *Chem. Rev.* **116**, 12785–12820 (2016).
42. R. Awatramani, P. Soriano, C. Rodriguez, J. J. Mai, S. M. Dymecki, Cryptic boundaries in roof plate and choroid plexus identified by intersectional gene activation. *Nat. Genet.* **35**, 70–75 (2003).
43. R. Lin *et al*., Cell-type-specific and projection-specific brain-wide reconstruction of single neurons. *Nat. Methods* **15**, 1033–1036 (2018).